Spin- and valley-resolved tunneling magnetoresistance in a ferromagnetic transition metal dichalcogenide planar heterojunction modulated by polarized light

Laipeng Luo and Shengxiang Wang

Department of Physics and State Key Laboratory of Low-Dimensional Quantum Physics,
Tsinghua University, Beijing 100084, People's Republic of China

Jun Zheng

College of Physics Science and Technology, Bohai University, Jinzhou 121013, People's Republic of China

Yong Guo[*]

Department of Physics and State Key Laboratory of Low-Dimensional Quantum Physics,
Tsinghua University, Beijing 100084, People's Republic of China

We propose a ferromagnetic planar heterojunction $MoSe_2/WSe_2/MoSe_2$, and theoretically explore the quantum transport modulated by off-resonant circular polarized light. We find that fully spin- and valley-polarized transport can be realized in both P (parallel) and AP (antiparallel) magnetization configurations. Specifically, the spin polarization can be reversed by switching the helicity of circular polarized light, while the valley polarization can be significantly modulated by changing magnetization configurations, and it's easier to reverse the valley polarization in the antiparallel configuration than that in the parallel configuration. Moreover, we demonstrate that the tunneling magnetoresistance (TMR) in the planar heterojunction can be modulated due to the spin-valley-dependent effective potential induced by optical modulation and band offset. Especially, the negative TMR is realized in strongly asymmetric magnetization configuration, which is contributed by specific spin- and valley-polarized states, and the sign of TMR can be switched by adjusting optical modulation intensity. This work may shed light on promising applications of spin-valley or TMR devices based on monolayer transition-metal dichalcogenide (TMDC) planar heterojunctions.

I. INTRODUCTION

Recently, transition-metal dichalcogenides (TMDCs) have attracted much attention because of their promising application for next-generation devices [1–4]. There are two inequivalent valleys located at the corners of the hexagonal Brillouin zone in TMDCs, which restricts the intervalley scattering without considering the phonon process [5,6]. Especially, in monolayer TMDCs, the broken inversion symmetry together with spin-orbital coupling (SOC) lead to strong spin-valley coupling [7], known as spin-valley locking, where the spin splitting of the valence bands is opposite at the two valleys due to the time-reversal symmetry [8]. Therefore, TMDCs are an ideal material platform for research on spin and valley physics.

Manipulation of electrons with a specific spin or valley is an important topic in the fields of spintronics and valleytronics. Due to broken inversion symmetry, monolayer TMDCs exhibit valley-dependent optical interband excitation, where circularly polarized light (CPL) with different helicity selectively excites electrons in different valleys [9]. Several research proposals have been raised based on mono-

layer TMDCs. For example, quantum spin and valley Hall effects are predicted in off-resonant CPL-illuminated MoS_2 [10]. In addition, valley-polarized transport has been observed successfully in optically pumped MoS_2 [11–13]. As with the cases in graphene, spin and valley filter/valve based on WSe_2 heterostructures have also been theoretically proposed [14]. On the other hand, tunneling magnetoresistance (TMR) of magnetic tunnel junctions is another key topic of concern due to its application in storage and magnetic sensor technologies [15]. The TMR effect and quantum transport have been theoretically and experimentally investigated in several kinds of two-dimensional (2D) materials through a ferromagnetic junction, such as graphene [16,17], silicene [18–20], and phosphorene [21]. Most recently, spin-valley-dependent transport and TMR have been explored in a ferromagnetic MoS_2 junction with a quantum well [22] and an asymmetrical MoS_2 or $MoSe_2$ tunnel junction [23,24].

A planar heterojunction (PH) is an important kind of two-dimensional material heterostructure, in which different atomic panels are combined in a single atomic layer due to the similar structure and relatively little lattice mismatch. TMDCs with 2H phase (for example, MX_2, M = Mo/W, X = S/Se) are very similar in their atomic structure, so the planar heterojunctions can share atomically flat interfaces, where a localized edge state will be emerged because of the
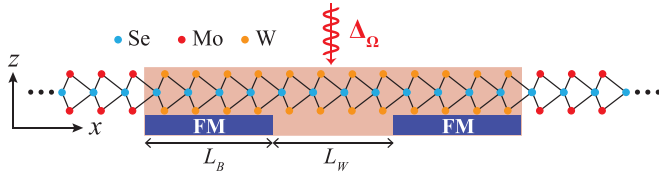
---
[*]guoy66@tsinghua.edu.cn

FIG. 1. Schematic diagram of the ferromagnetic MoSe$_2$/WSe$_2$/MoSe$_2$ planar heterojunction. Orange and red spheres represent W and Mo atoms, respectively, while the blue ones represent Se atoms. There are two magnetic regions with length L_B on both sides of the WSe$_2$ region. The whole WSe$_2$ region is illuminated by the off-resonant circularly polarized light.

hybridization of orbitals [25]. Band offset [26,27] between different components of PHs can be utilized to modify the electronic properties, which makes them valuable in the design of potential functional devices, such as photoelectric [28] and thermoelectric devices [29]. Atomically flat TMDC PHs have been successfully synthesized by several experimental groups since 2014 [30–32], which can be divided into three categories: (i) PHs with shared M atom, such as MoS$_2$/MoSe$_2$; (ii) PHs with common X atom, like MoS$_2$/WS$_2$; and (iii) PHs with different M and X atoms. In the experimental research [33], it has been demonstrated that PHs with common X atoms have the smallest lattice mismatch (<1%), where the effect of strain on the interface can be neglected. In contrast, in the PHs with different X atoms, the lattice mismatch is about 4%, which leads to sizable strain and the lattice relaxation effects should be considered. In this work, we focus on the planar heterojunctions with shared X atoms (MoSe$_2$/WSe$_2$/MoSe$_2$), so the boundary conditions adopted in our model is reasonable.

Previous research on quantum transport and the TMR effect mentioned above are all based on the junction composed of the same material. While for planar heterojunctions composed by different TMDC materials [27,34], there is little research on TMR effects yet. In this work, we proposed a magnetic tunneling junction based on TMDC planar heterojunctions. Without losing generality, we choose the MoSe$_2$/WSe$_2$/MoSe$_2$ heterojunctions for concrete numerical calculations. It can be demonstrated that the band offset and CPL-induced gap result in spin- and valley-resolved effective potential; electrons with different spin and valley indices experience different barrier or well when tunneling through the heterojunctions, which leads to fully spin- and valley-polarized transport. Different from the previous work, we find that both the spin and valley polarization can be reversed by magnetic and off-resonant light modulations, regardless of the magnetization configurations. Surprisingly, the negative TMR can be achieved in the strongly asymmetric magnetization cases when the CPL intensity goes over a critical point. It is found that this negative TMR is strongly associated with the specific spin- and valley-polarized states, which has not been reported in the previous related work.

II. MODEL AND METHODS

Figure 1 shows the schematic diagram of the ferromagnetic planar heterojunction we designed. On both sides of the WSe$_2$

region, there are two ferromagnetic modulation regions. The exchange splitting induced by the magnetic effect is m_1 and m_2, respectively. The entire WSe$_2$ region is illuminated by off-resonant circular polarized light. The heterojunctions can be divided into two types of configurations: P (parallel) and AP (antiparallel) according to the magnetization orientations of the two FM regions. Throughout the paper, we assumed that the magnetization orientation in the first FM region is always positive ($m_1 > 0$), while in the second FM region can be reversed.

In this context, we use $\uparrow$ and $\downarrow$ to represent electrons with spin up and spin down, respectively, K and K' for those with different valleys. For the pristine cases, the low-energy effective Hamiltonian of monolayer TMDCs can be described by [7]

$$\hat{H} = a\tau(\eta k_x \hat{\sigma}_x + k_y \hat{\sigma}_y) + \frac{\Delta}{2}\hat{\sigma}_z - \lambda\eta\frac{\hat{\sigma}_z - 1}{2}\hat{s}_z, \quad (1)$$

where σ_i is the Pauli matrix, a is the lattice constant, and τ is the coupling between the states at the band extrema in the k·p approximation. 2λ is the spin splitting at the valence band top caused by the SOC, and Δ is the energy gap. $s_z = 1(-1)$ represents spin up (down) electrons, and $\tau = 1(-1)$ corresponds to $K(K')$ valleys. The circularly polarized light can be described by an electromagnetic potential as A(t)=[Asin(±Ωt), Acos(±Ωt)], where A and Ω correspond to the amplitude of potential and frequency of light, respectively. According to the Floquet theory [35], when $\hbar\Omega \gg t$, the effect of time-dependent electromagnetic potential on the system can be reduced to an effective static Hamiltonian. The circularly polarized light does not directly excite the electrons and instead effectively modifies the electronic structure through virtual photon absorption and emission processes [36,37]. For $eAv_f/\hbar\Omega \ll 1$, effective static Hamiltonian near the Dirac point can be written as $\pm\eta\Delta\Omega\sigma_z$, where $\Delta\Omega$ is the effective energy term describing the intensity of the CPL. The magnetic modulation can be induced via the magnetic proximity effect or magnetic doping [38]; its contribution to the Hamiltonian can be simply written by $-m\hat{s}_z$, where m represents the exchange splitting. Therefore, in the proposed cases, the effective Hamiltonian is

$$\hat{H} = a\tau(\eta k_x \hat{\sigma}_x + k_y \hat{\sigma}_y) + \frac{\Delta}{2}\hat{\sigma}_z - \lambda\eta\frac{\hat{\sigma}_z - 1}{2}\hat{s}_z$$
$$+ \eta\Delta\Omega\hat{\sigma}_z - m(x)\hat{s}_z, \quad (2)$$

where $\Delta\Omega = \pm(eAv_f)^2/\hbar\Omega$ and $\pm$ correspond to the right- and left-handed circularly polarized light, respectively. The general form of wave functions in each region is

$$\Psi(x) = a\begin{pmatrix} 1 \\ \sqrt{K_c/K_v}e^{i\eta\theta} \end{pmatrix}e^{ik_x x}e^{ik_y y}$$
$$+ b\begin{pmatrix} 1 \\ -\sqrt{K_c/K_v}e^{-i\eta\theta} \end{pmatrix}e^{-ik_x x}e^{ik_y y}, \quad (3)$$

$$K_c K_v = k_x^2 + k_y^2 = \mathbf{k}^2. \quad (4)$$

Here we define $K_c = (E - E_c + ms_z - \eta\Delta\Omega)/\eta a\tau$ and $K_v = (E - E_v + ms_z + \eta\Delta\Omega - \lambda\eta s_z)/\eta a\tau$, E_c (E_v) is the energy of conduction (valence) band minimum (maximum) in the absence of CPL and spin-orbit coupling. θ is the angle of

incidence electron wave vector **k** relative to x axis. The wave functions in the jth region from Eq. (3) can be rewritten by

$$\Psi_j(x) = R_j(x)\begin{pmatrix} a_j \\ b_j \end{pmatrix} e^{ik_y y}, \tag{5}$$

where

$$R_j(x) = \begin{pmatrix} e^{ik_x x} & e^{-ik_x x} \\ \sqrt{K_c/K_v}e^{i\eta\theta}e^{ik_x x} & -\sqrt{K_c/K_v}e^{-i\eta\theta}e^{-ik_x x} \end{pmatrix}. \tag{6}$$

Using the continuity of the wave function at the boundaries of each region ($x = 0$, L_B, $L_B + L_W$, and $2L_B + L_W$), the recursive relations of coefficients are obtained:

$$\begin{pmatrix} a_{j+1} \\ b_{j+1} \end{pmatrix} = R_{j+1}^{-1}R_j\begin{pmatrix} a_j \\ b_j \end{pmatrix} = M_j\begin{pmatrix} a_j \\ b_j \end{pmatrix}, \tag{7}$$

$$\begin{pmatrix} 0 \\ t_{\eta,s} \end{pmatrix} = \prod_j M_j\begin{pmatrix} 1 \\ r_{\eta,s} \end{pmatrix} = M_t\begin{pmatrix} 1 \\ r_{\eta,s} \end{pmatrix}. \tag{8}$$

The spin- and valley-resolved transmission probability can be calculated through the transfer-matrix method [39] $T_{\eta,s} = |t_{\eta,s}|^2$, where the transmission coefficient $t_{\eta,s}$ can be derived from the elements of M_t in Eq. (8). The conductance at zero temperature is given by the Landauer-Büttiker formula [40]

$$G_{\eta,s} = G_0 \int T_{\eta,s}\cos\theta \, d\theta, \tag{9}$$

where $G_0 = 2e^2/h$ is the quantum conductance. Conductance of specific spin and valley indices are denoted by $G_{\uparrow,K}$, $G_{\uparrow,K'}$, $G_{\downarrow,K}$, $G_{\downarrow,K'}$, respectively. The valley-resolved and total conductance are

$$G_{K(K')} = \frac{G_{\uparrow,K(K')} + G_{\downarrow,K(K')}}{2}, \tag{10}$$

$$G_t = G_K + G_{K'}, \tag{11}$$

and the spin (valley) polarization is defined as

$$P_{S(V)} = [G_{\uparrow(K)} - G_{\downarrow(K')}]/G_t. \tag{12}$$

Finally, the TMR can be derived by

$$\text{TMR} = \frac{G_P - G_{AP}}{G_P}. \tag{13}$$

III. RESULTS AND DISCUSSION

A. Band structure

From Eq. (4), we can derive the energy dispersion of WSe$_2$ and MoSe$_2$ with CPL as

$$2E = \pm\sqrt{(2ka\tau)^2 + (E_c - E_v - \lambda\eta s + 2\eta\Delta\Omega)^2} + E_c + E_v + \lambda\eta s - 2ms.$$

The effective energy of CPL $\Delta\Omega$ is coupled with valley index η in the dispersion. Figures 2(a) and 2(b) show the modification of the band structure of monolayer TMDC under magnetic and optical modulations. The conduction band of K electrons moves to a high energy level when illuminated by right-handed CPL, while that of spin up electrons move to lower energy when the magnetic orientation is positive. As a result, the CBM in modulated regions changes to $E_c =$
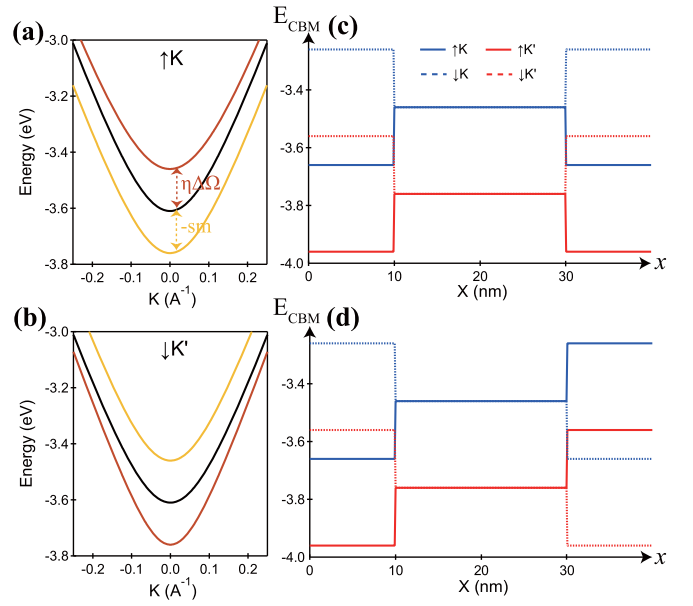
FIG. 2. Band structure of $\uparrow, K$ (a) and $\downarrow, K'$ (b) branches with optical and magnetic modulations, the black line denotes the pristine band, while the red and yellow lines represent the bands modulated by the off-resonant CPL and magnetic effect, respectively; (c) and (d) Spin- and valley- resolved conduction band minimum (CBM) energy in the planar heterojunctions. The CBMs are determined with respect to the vacuum level [27].

$E_c + \eta\Delta\Omega - ms$ [see Figs. 2(c) and 2(d)]. In particular, when $\Delta\Omega > \Delta\Omega_c = Ec_{WSe_2} - Ec_{MoSe_2}$, the CPL-induced energy shift flips the pristine band offset, so the effective potentials in the WSe$_2$ region are spin and valley dependent, which leads to unique transport properties when electrons are tunneling through them.

B. Transmission and conductance

In this section, we investigate the spin- and valley-resolved transport of the heterojunctions with P and AP configurations, respectively. First, we consider cases where $|m_1|$ is quantitatively equal to $|m_2|$. Figure 3 shows the contour plot of spin-valley-dependent transmission probability with respect to θ and m in the two configurations. In all cases, the incident angle is limited within 30° due to the band offset. Interestingly, in the P configuration, the allowed incident angles for spin up branches are smaller than that for spin down branches, while in the AP configuration, the allowed incident angle for K' valley is larger than that for K valley. In the P configuration, the cutoff points of m for $T_{\uparrow,\eta}$ are $Ec_{WSe_2} - E_F + \eta\Delta\Omega$, while those for $T_{\downarrow,\eta}$ are $E_F - Ec_{WSe_2} - \eta\Delta\Omega$. However, the cutoff points in the P configuration are $\pm|Ec_{WSe_2} - E_F + \eta\Delta\Omega|$, which are symmetrical and only dependent on the valley index.

Figures 4(a1)–4(a4) show the spin- and valley-resolved conductance as a function of $\Delta\Omega$ in P configuration. With enhanced right-handed CPL intensity, G_K is gradually suppressed, while $G_{K'}$ increases. Notably, when the exchange splitting is relatively large ($m > E_F - Ec_{WSe_2}$), $G_\downarrow$ is completely suppressed in the absence of CPL, because the
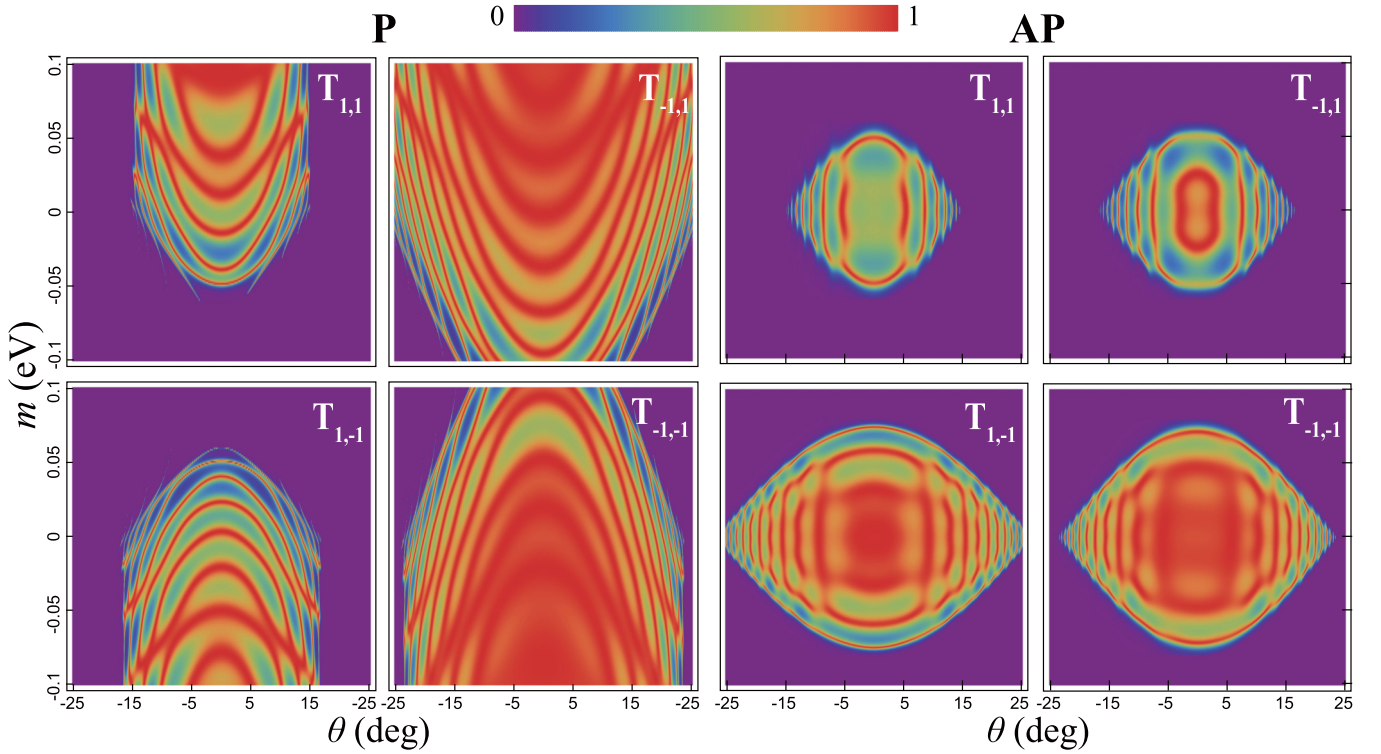
FIG. 3. Contour plot of transmission probability with respect to θ and m. Left panel: Spin- and valley-resolved transmission in the P configuration. Right panel: Spin- and valley-resolved transmission in the AP configuration. $\Delta\Omega = 50$ meV for all cases.

effective barriers in the FM regions are higher than Fermi energy. While $G_\downarrow$ recovers gradually with $\Delta\Omega$ increasing, the CPL-induced energy shift reduces the height of the effective barriers in FM regions [see Figs. 4(a2) and 4(a4)]. Interestingly, when the intensity of the left-handed CPL increases, $G_\downarrow$ exceeds $G_\uparrow$, which leads to the reversal of spin polarization. However, when modulated by the right-handed CPL, $G_\uparrow$ is always higher than $G_\downarrow$. In Figs. 4(b1) and 4(b2), we present

the relationship between $G_{\eta,s}$ and the exchange splitting m. It can be seen that when m increases, the conductance tends to stabilize at a finite value, and the height of effective barrier in this case is only dependent on the effective potential in the nonmagnetic region, which is determined by $\Delta\Omega$, so the transport of the K electrons is greatly suppressed with increasing $\Delta\Omega$. However, things are quite different in the AP configuration. While the CPL intensity is relatively weak, the
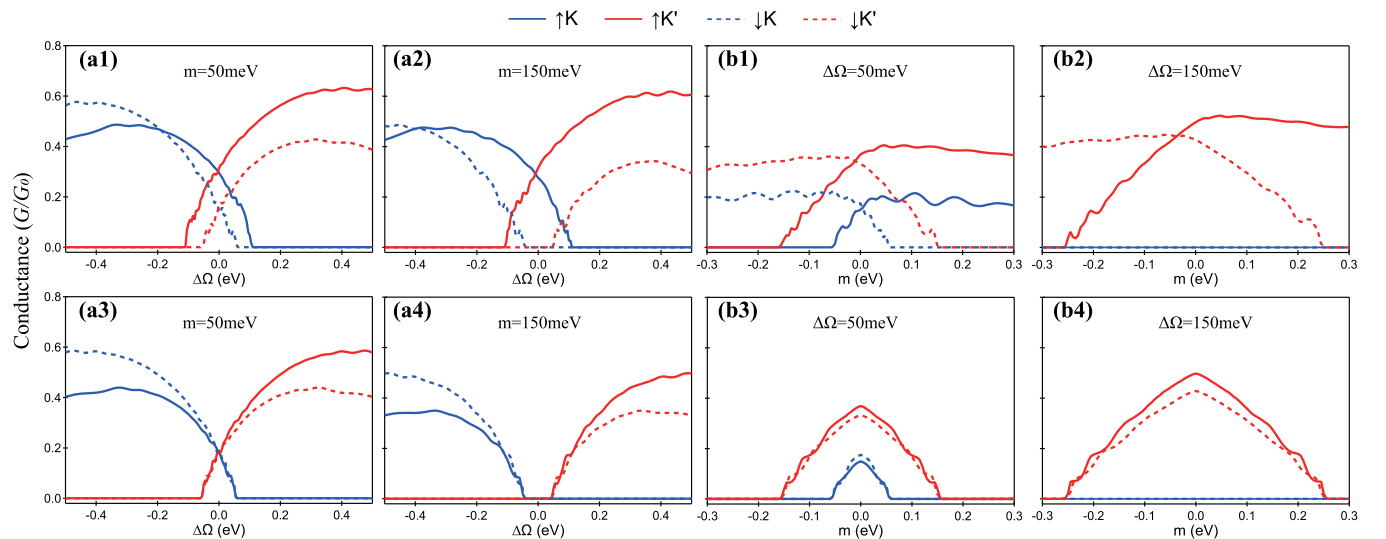

FIG. 4. Spin- and valley-resolved conductance of the heterojunctions. (a1)−(a4) Conductance with respect to $\Delta\Omega$. Energy is fixed at 905 meV above Fermi energy. (b1)−(b4) Conductance as a function of magnetic strength m. In the top row, the heterojunction is P configuration, and AP configuration in the bottom row. m_1 is set quantitatively equal to m_2 in all cases.
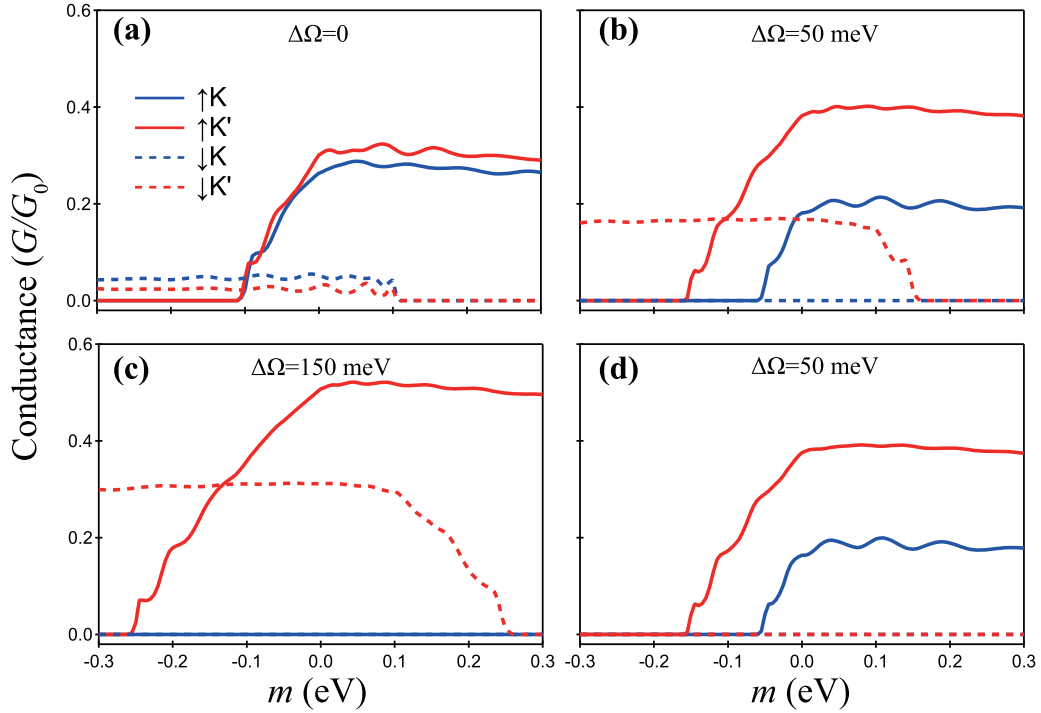
FIG. 5. Spin- and valley-polarized conductance of the heterojunctions under different $\Delta\Omega$ with fixed m_1. (a)–(c) $m_1 = 100$ meV, and $m_1 = 200$ meV in (d).

transport of all the branches of electrons is almost degenerate, as shown in Figs. 4(a3) and 4(a4). In Figs. 4(b3) and 4(b4), the transport is limited within a finite interval of m, whatever the CPL intensity. Next, we fix the magnetization strength in the first FM region to explore the effect of m_2 on the quantum transport of planar heterojunctions. It can be seen in Fig. 5(a) that without CPL, only when $|m_2| < E_F - Ec_{WSe_2}$ can all the branches of electrons tunnel through the junction. However, the $G_\downarrow$ is significantly lower than the $G_\uparrow$, which is quite different from that in Fig. 4(b1). This can be ascribed to the asymmetric effective potential barriers in the two FM regions. When the CPL modulation is applied, the transport of electrons with different valleys is distinguished. For K electrons with spin down, the right-handed CPL raises the effective potential barrier in the first FM region. When the height of the effective barrier exceeds the Fermi energy, the transport of the corresponding branch of electrons will be completely suppressed, as shown in Fig. 5(b). As $\Delta\Omega$ increases, the potential barrier for K, $\uparrow$ electrons is also raised, where only K' electrons can tunnel through the junctions [see Fig. 5(c)]. Therefore, the competition between optical and magnetic modulation results in asymmetric spin- and valley-resolved effective potential barriers. The quantum transport properties of the proposed heterojunctions can be modulated by specifically designing the strength and orientation of m and $\Delta\Omega$.

C. Polarization and TMR effect

Furthermore, we investigate the spin- and valley-polarized transport of TMDC PHs under magnetic and optical modulations. As can be seen in Fig. 6(a), perfect spin polarization

is realized when $|m_2|$ is large enough, the critical points are $\pm|E_F - Ec_{WSe_2} + |\Delta\Omega||$, and the trend of P_s versus m_2 is almost independent of the optical modulation. Surprisingly, the CPL modulation can also reverse the P_s, regardless of the magnetic configuration [see Fig. 6(c)]. P_s in the P configuration is more sensitive to the magnetization than that in the AP configuration, which is originated from the degenerate transport in AP configuration [see Figs. 4(a3) and 4(a4)]. However, cases for valley polarization P_v are quite different. For AP configurations, when $|m_2|$ is large enough, the heterojunction exhibits perfect valley polarization, where only one branch of electrons participate in the transport and the polarization direction depends on the helicity of the optical field [see Fig. 6(b)]. While for the P configuration, P_v gradually decreases and tends to stabilize at a finite value. Figure 6(d) shows valley polarization as a function of $\Delta\Omega$ in the two configurations. It can be seen that the relationships between valley polarization and $\Delta\Omega$ are similar in the two configurations. For the AP configuration, the CPL intensity required to reverse P_v is weaker than that for the P configuration, which means valley polarization of planar heterojunctions in AP configuration is easier to be controlled, so they may be suitable for valley filter applications.

We also explore the TMR effect in this system. First, we investigate the total conductance G_t as a function of $\Delta\Omega$ in the two configurations. As can be seen in Fig. 7(a), both G_P and G_{AP} decrease when m_2 increased, because there are less branches of electrons contributing to the transport as m_2 increased. Interestingly, when m_2 is weak, G_P is always higher than G_{AP}, which means that the TMR of the system is always positive. However, when m_2 is relatively strong, G_{AP} will be higher than G_P when $\Delta\Omega$ exceed a critical point, which will lead to a negative TMR [see the black line in
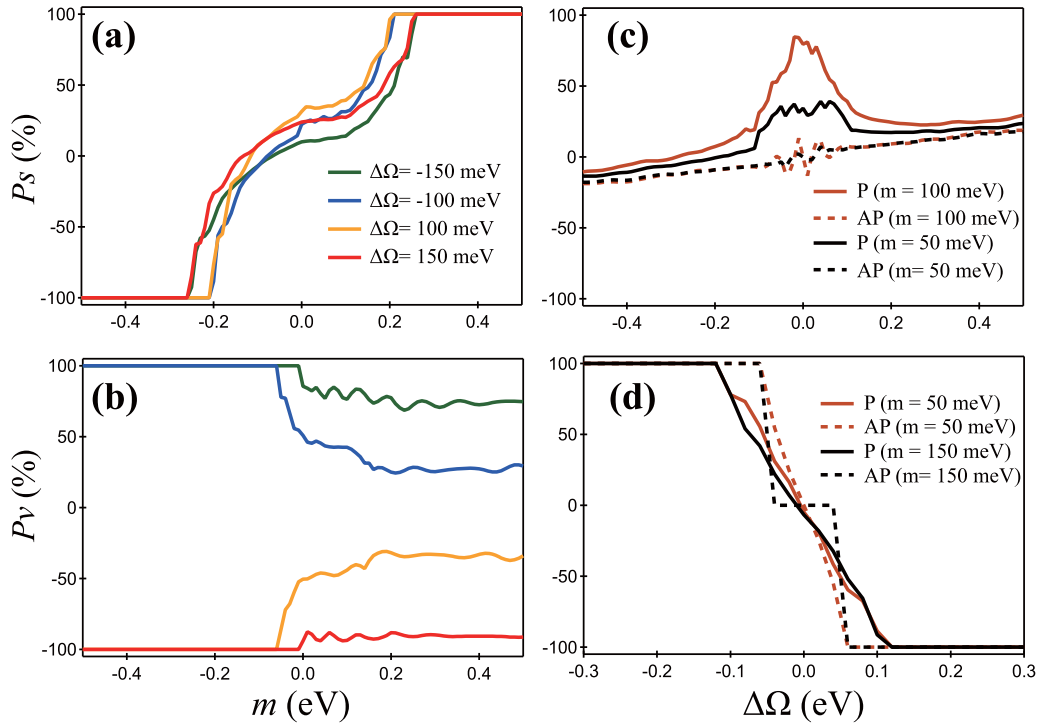
FIG. 6. Spin- and valley-polarization of the planar heterojunctions. P_s (a) and P_v (b) with respect to m_2 (m_1 is fixed at 100 meV); (c) and (d) P_s and P_v as a function of $\Delta\Omega$.

Fig. 6(b)]. Therefore, both the strength and sign of TMR can be optically modulated by off-resonant CPL in an asymmetric ferromagnetic TMDC planar heterojunction. Figures 7(e) and 7(f) show the effective potential in the positive and negative TMR cases, respectively. In both cases, electrons experience an effective quantum well and step potential. It can be seen that for the cases of positive TMR, both G_P and G_{AP} are contributed by $G_{\uparrow,\downarrow,K}$, which means the transport states are just valley-polarized. However, for the cases of negative TMR, G_P is only contributed by $G_{\uparrow,K}$, and G_{AP} is contributed by $G_{\downarrow,K}$, which means that the negative TMR is resulted from the

same valley-polarized states with different spin polarization. This is a new finding which has not been reported by previous related research. We further study the effect of the length of modulation regions on G_t and TMR. Although the amplitude of oscillation is relatively small, it still can be clearly seen that the total conductance oscillates with L_W. The oscillatory behavior of the conductance curve is due to the Fabry-Perot resonance, which can be ascribed to wavevector quantization. The amplitudes of these oscillations are relatively small, which is resulted from the shallow quantum well in the effective potential [see Figs. 7(e) and 7(f)].
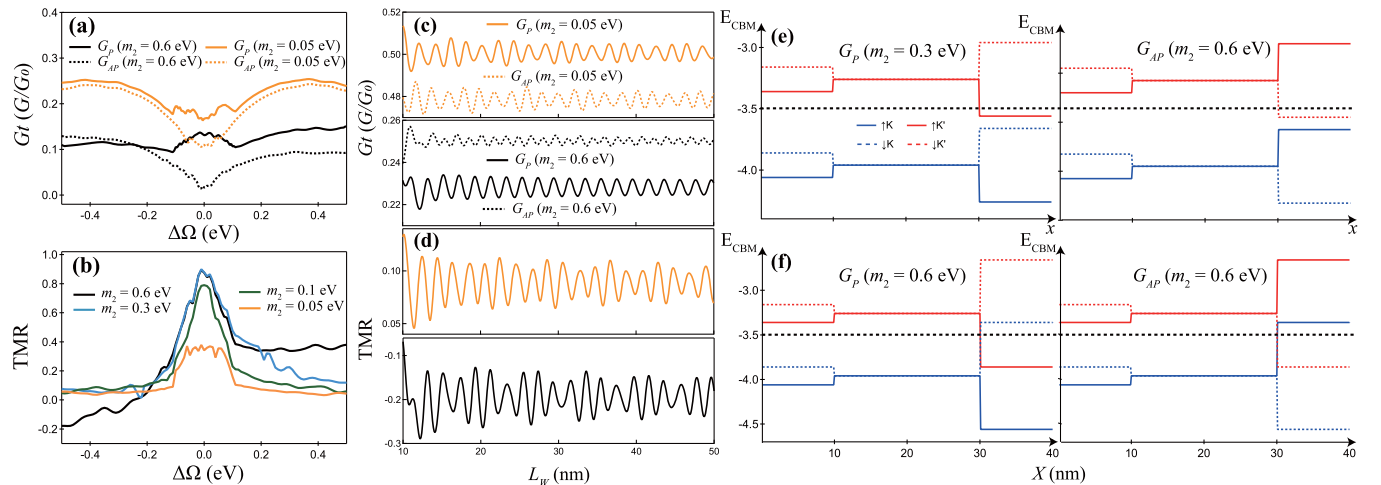

FIG. 7. Total conductance G_t with different magnetic configurations and TMR effect in the heterojunctions. G_t (a) and TMR (b) with respect to $\Delta\Omega$. (c) and (d) G_t and TMR with respect to L_W. (e) and (f) Spin- and valley- resolved conduction band minimum (CBM) energy in the cases of positive and negative TMR, respectively. The dotted black lines denote the Fermi energy. $\Delta\Omega = -350$ meV in (c)–(f).

IV. CONCLUSION

In summary, we propose an optically modulated ferromagnetic tunnel junction based on planar heterojunctions composed by different TMDC materials. Spin- and valley-resolved transport in the two different magnetic configurations and the TMR effect are theoretically investigated by numerical calculations. Due to the strong SOC in monolayer TMDCs, the band offset and off-resonant CPL contribute to the spin- and valley-resolved effective potential, which leads to the fully spin- and valley-polarized transport. Interestingly, the spin polarization can be reversed by both magnetic and optical modulation, regardless of the magnetization configurations. It is found that the CPL intensity required to reverse the P_v in the AP configuration is lower than that in the P configuration. On the other hand, the TMR in the planar heterojunction can be optically modulated due to the spin-valley-dependent effective potential. When $|m_2|$ is relatively weak, G_P is always higher than G_{AP}, leading to the positive TMR. However, when $|m_2|$ is relatively strong, G_{AP} goes over G_P at a critical $\Delta\Omega$, which results in a transition of TMR from positive to negative. Especially, it is found that the negative TMR is contributed by specific spin- and valley-polarized states, and the sign of TMR can be switched by changing the CPL intensity. Our work may be useful for research on spintronics or valleytronics and TMR devices based on TMDC planar heterojunctions.

[1] K. S. Novoselov, D. Jiang, F. Schedin, T. J. Booth, V. V. Khotkevich, S. V. Morozov, and A. K. Geim, Two-dimensional atomic crystals, Proc. Natl. Acad. Sci. USA **102**, 10451 (2005).

[2] C. Lee, Q. Li, W. Kalb, X. Z. Liu, H. Berger, R. W. Carpick, and J. Hone, Frictional characteristics of atomically thin sheets, Science **328**, 76 (2010).

[3] A. Splendiani, L. Sun, Y. Zhang, T. Li, J. Kim, C.-Y. Chim, G. Galli, and F. Wang, Emerging photoluminescence in monolayer MoS$_2$, Nano Lett. **10**, 1271 (2010).

[4] K. F. Mak, C. Lee, J. Hone, J. Shan, and T. F. Heinz, Atomically Thin MoS$_2$: A New Direct-Gap Semiconducto, Phys. Rev. Lett. **105**, 136805 (2010).

[5] T. Li and G. Galli, Electronic properties of MoS$_2$ nanoparticles, J. Phys. Chem. C **111**, 16192 (2007).

[6] S. Lebègue and O. Eriksson, Electronic structure of two-dimensional crystals from ab initio theory, Phys. Rev. B **79**, 115409 (2009).

[7] D. Xiao, G. B. Liu, W. Feng, X. Xu, and W. Yao, Coupled Spin and Valley Physics in Monolayers of MoS$_2$ and Other Group-V Dichalcogenides, Phys. Rev. Lett. **108**, 196802 (2012).

[8] Z. Y. Zhu, Y. C. Cheng, and U. Schwingenschlögl, Giant spin-orbit-induced spin splitting in two-dimensional transition-metal dichalcogenide semiconductors, Phys. Rev. B **84**, 153402 (2011).

[9] K. Hao, G. Moody, F. Wu, C. K. Dass, L. Xu, C. H. Chen, L. Sun, M.-Y. Li, L.-J. Li, A. H. MacDonald, and X. Li, Direct measurement of exciton valley coherence in monolayer WSe$_2$, Nat. Phys. **12**, 677 (2016).

[10] M. Tahir, A. Manchon, and U. Schwingenschlögl, Photoinduced quantum spin and valley Hall effects, and orbital magnetization in monolayer MoS$_2$, Phys. Rev. B **90**, 125438 (2014).

[11] T. Cao, G. Wang, W. Han, H. Ye, C. Zhu, J. Shi, Q. Niu, P. Tan, E. Wang, B. Liu, and J. Feng, Valley-selective circular dichroism of monolayer molybdenum disulphide, Nat. Commun. **3**, 887 (2012).

[12] K. F. Mak, K. He, and T. F. Heinz, Control of valley polarization in monolayer MoS$_2$ by optical helicity, Nat. Nanotechnol. **7**, 494 (2012).

[13] H. Zeng, J. Dai, W. Yao, D. Xiao, and X. Cui, Valley polarization in MoS$_2$ monolayers by optical pumping, Nat. Nanotechnol. **7**, 490 (2012).

[14] D. Liu, B. Liu, R. Yuan, J. Zheng, and Y. Guo, Valley filter and valley valve based on WSe$_2$ double-barrier junctions modulated by polarized light, Phys. Rev. B **103**, 245432 (2021).

[15] J. S. Moodera, L. R. Kinder, T. M. Wong, and R. Meservey, Large Magnetoresistance at Room Temperature in Ferromagnetic Thin Film Tunnel Junctions, Phys. Rev. Lett. **74**, 3273 (1995).

[16] J. Zou, G. Jin, and Y. qiang Ma, Negative tunnel magnetoresistance and spin transport in ferromagnetic graphene junctions, J. Phys.: Condens. Matter **21**, 126001 (2009).

[17] C. Bai and X. Zhang, Large oscillating tunnel magnetoresistance in ferromagnetic graphene single tunnel junction, Phys. Lett. A **372**, 725 (2008).

[18] R. Saxena, A. Saha, and S. Rao, Conductance, valley and spin polarizations, and tunneling magnetoresistance in ferromagnetic-normal-ferromagnetic junctions of silicene, Phys. Rev. B **92**, 245412 (2015).

[19] D. Wang, Z. Huang, Y. Zhang, and G. Jin, Spin-valley filter and tunnel magnetoresistance in asymmetrical silicene magnetic tunnel junctions, Phys. Rev. B **93**, 195425 (2016).

[20] Y. Hajati and Z. Rashidian, Valley and spin resonant tunneling current in ferromagnetic/nonmagnetic/ferromagnetic silicene junction, AIP Adv. **6**, 025307 (2016).

[21] M. Zare, L. Majidi, and R. Asgari, Giant magnetoresistance and anomalous transport in phosphorene-based multilayers with noncollinear magnetization, Phys. Rev. B **95**, 115426 (2017).

[22] W.-T. Lu, H.-Y. Tian, H.-M. Liu, Y.-F. Li, and W. Li, Spin- and valley-dependent negative magnetoresistance in a ferromagnetic MoS$_2$ junction with a quantum well, Phys. Rev. B **98**, 075405 (2018).

[23] X.-J. Qiu, Z.-Z. Cao, J. Hou, and C.-Y. Yang, Controlled giant magnetoresistance and spin-valley transport in an asymmetrical MoS$_2$ tunnel junction, Appl. Phys. Lett. **117**, 102401 (2020).

[24] Y. Hajati, M. Alipourzadeh, and I. Makhfudz, Spin- and valley-polarized transport and magnetoresistance in asymmetric

ferromagnetic WSe$_2$ tunnel junctions, Phys. Rev. B **103**, 245435 (2021).

[25] O. Ávalos-Ovando, D. Mastrogiuseppe, and S. E. Ulloa, Lateral interfaces of transition metal dichalcogenides: A stable tunable one-dimensional physics platform, Phys. Rev. B **99**, 035107 (2019).

[26] J. Kang, S. Tongay, J. Zhou, J. Li, and J. Wu, Band offsets and heterostructures of two-dimensional semiconductors, Appl. Phys. Lett. **102**, 012111 (2013).

[27] H. Ghadiri and A. Saffarzadeh, Band-offset-induced lateral shift of valley electrons in ferromagnetic MoS$_2$/WS$_2$ planar heterojunctions, J. Appl. Phys. **123**, 104301 (2018).

[28] J. Lee, J. Huang, B. G. Sumpter, and M. Yoon, Strain-engineered optoelectronic properties of 2D transition metal dichalcogenide lateral heterostructures, 2D Mater. **4**, 021016 (2017).

[29] Z. Zhang, Y. Xie, Q. Peng, and Y. Chen, A theoretical prediction of super high-performance thermoelectric materials based on MoS$_2$/WS$_2$ hybrid nanoribbons, Sci. Rep. **6**, 21639 (2016).

[30] X. Duan, C. Wang, J. C. Shaw, R. Cheng, Y. Chen, H. Li, X. Wu, Y. Tang, Q. Zhang, A. Pan, J. Jiang, R. Yu, Y. Huang, and X. Duan, Lateral epitaxial growth of two-dimensional layered semiconductor heterojunctions, Nat. Nanotechnol. **9**, 1024 (2014).

[31] Y. Gong, J. Lin, X. Wang, G. Shi, S. Lei, Z. Lin, X. Zou, G. Ye, R. Vajtai, B. I. Yakobson, H. Terrones, M. Terrones, B. K. Tay, J. Lou, S. T. Pantelides, Z. Liu, W. Zhou, and P. M. Ajayan, Vertical and in-plane heterostructures from WS$_2$/MoS$_2$ monolayers, Nat. Mater. **13**, 1135 (2014).

[32] K. Chen, X. Wan, W. Xie, J. Wen, Z. Kang, X. Zeng, H. Chen, and J. Xu, Lateral built-in potential of monolayer MoS$_2-$WS$_2$ in-plane heterostructures by a shortcut growth strategy, Adv. Mater. **27**, 6431 (2015).

[33] C. Zhang, M. Y. Li, J. Tersoff, Y. Han, Y. Su, L. J. Li, D. A. Muller, and C. K. Shih, Strain distributions and their influence on electronic structures of WSe$_2$MoS$_2$ laterally strained heterojunctions, Nat. Nanotechnol. **13**, 152 (2018).

[34] L. Luo, S. Wang, and Y. Guo, Optically Controlled Valley Filter and Transistor Based on Transition-Metal Dichalcogenide Planar Heterojunctions, Phys. Rev. Appl. **18**, 044020 (2022).

[35] B. Dóra, J. Cayssol, F. Simon, and R. Moessner, Optically Engineering the Topological Properties of a Spin Hall Insulator, Phys. Rev. Lett. **108**, 056602 (2012).

[36] M. Ezawa, Photoinduced Topological Phase Transition and a Single Dirac-Cone State in Silicene, Phys. Rev. Lett. **110**, 026603 (2013).

[37] T. Kitagawa, T. Oka, A. Brataas, L. Fu, and E. Demler, Transport properties of nonequilibrium systems under the application of light: Photoinduced quantum Hall insulators without Landau levels, Phys. Rev. B **84**, 235108 (2011).

[38] B. Scharf, G. Xu, A. Matos-Abiague, and I. Žutić, Magnetic Proximity Effects in Transition-Metal Dichalcogenides: Converting Excitons, Phys. Rev. Lett. **119**, 127403 (2017).

[39] David Yuk Kei Ko and J. C. Inkson, Matrix method for tunneling in heterostructures: Resonant tunneling in multilayer systems, Phys. Rev. B **38**, 9945 (1988).

[40] M. Büttiker, Four-Terminal Phase-Coherent Conductance, Phys. Rev. Lett. **57**, 1761 (1986).